Infrared Physics & Technology 52 (2009) 89–96

Contents lists available at ScienceDirect

Infrared Physics & Technology

journal homepage: www.elsevier.com/locate/infrared

Infrared dipole-coupled bolometer response on a hemispherical silicon immersion lens

Brian A. Lail [a,*], Christopher T. Middlebrook [b], Peter M. Krenz [c], Glenn D. Boreman [c]

[a] Florida Institute of Technology, Department of Electrical and Computer Engineering, 150 W. University Blvd., Melbourne, FL 32901, United States
[b] Michigan Technological University, Department of Electrical and Computer Engineering, 1400 Townsend Drive, Houghton, MI 49931, United States
[c] University of Central Florida, CREOL - The College of Optics and Photonics, 4000 Central Florida Blvd., Orlando, FL 32816, United States

ARTICLE INFO

Article history:
Received 24 July 2008
Available online 11 March 2009

Keywords:
Infrared antennas
Immersion lens
Antenna-coupled detectors

ABSTRACT

Response of an infrared (λ = 10.6 μm) dipole antenna-coupled bolometer fabricated at the center of the flat side of a hemispherical silicon immersion lens is presented. Predicted and measured antenna patterns as well as the ratio of power from the lens-side to the air-side are provided as a function of illumination F/#. The power-division ratio, Φ_{lens}/Φ_{air}, is shown to be given by the square root of the lens dielectric constant, $\epsilon_{Si}^{1/2} = 3.4$, for F/# larger than F/2 whereas as F/# decreases to F/1 the ratio increases to 5 due to off-axis features in the radiation pattern.

1. Introduction

Infrared antenna-coupled microbolometers are typically fabricated on planar dielectric substrates. Device excitation is provided by either air-side or substrate-side illumination [1]. Previous literature indicates that substrate-side illumination is the preferred method since an antenna on a dielectric will radiate preferentially into the dielectric half space [2]. A dipole antenna on the interface separating two dielectric half-spaces exhibits radiated power division $\Phi_1/\Phi_2 = (\varepsilon_1/\varepsilon_2)^{3/2}$, where Φ_1 and Φ_2 represent power radiated in the broadside direction into half-spaces of permittivity ε_1 and ε_2, respectively, indicating preferential radiation into the medium of higher refractive index [2,3]. Through reciprocity, the power received by the antenna favors the higher index medium by the same factor. For a dipole on a Si/air boundary, with $\varepsilon_2 = \varepsilon_{Si} = 11.7$ and $\varepsilon_1 = \varepsilon_{air} = 1$, the received power from the substrate-side in the broadside direction is 40 times that from the air-side. Problems such as reflection losses, a narrower reception-cone angle, and power loss to substrate modes arise when substrate side illumination is utilized with a slab dielectric. In order to eliminate or mitigate these problems an immersion lens is used [3]. A high-resistivity silicon (Si) immersion lens with a measured resistivity of 12.5 kΩ cm is chosen for its high transmission in the infrared as well as its compatibility with fabrication processes. A straightforward approach in using an immersion lens would be to place the lens directly in contact with the planar substrate, effectively sandwiching the antenna between the two media. Not withstanding its applicability in the millimeter wave range this approach allows for air gaps that give rise to reflections at infrared wavelengths. Index matching fluid is not readily available at the prescribed index n_{Si} = 3.4 at the required wavelengths. Additionally, alignment between the center of the lens and the antenna becomes very difficult at these scales due to the typical antenna dimensions which are on the order of a wavelength. To avoid these problems the antenna is fabricated directly on the flat side of an immersion lens [4]. This eliminates air-gap issues and the centering of the antenna can be done very accurately during the fabrication process.

In this paper, a dipole residing on the boundary between an air half-space and a 5-mm radius hemispherical Si lens is considered. Theoretical formulation is presented in Section 2 with a predicted broadside power division for lens-side versus air-side illumination accounting for the finite extent of the lens, as well as off-axis response. Then measured response at 10.6 μm from a dipole antenna on a Si lens is presented in Section 3, with broadside power division consistent with predictions made in Section 2. It should be noted that while the electromagnetic formulation is in terms of power quantities, device measurements yield a voltage which is proportional to the local irradiance in Watt/cm^2. The devices are thus described in terms of an irradiance responsivity in V/(W/cm^2).

2. Electromagnetic formulation

We consider a dipole located at the center of the flat surface of a high-resistivity hemispherical Si lens. The purpose is to determine the angular response for air-side and lens side illumination. Here we present an analytical formulation based on reciprocity which predicts the response as a function of incidence angle and illumination F/#, for both air-side and lens-side illumination.

* Corresponding author. Tel.: +1 321 674 8121; fax: +1 321 674 8192.
E-mail address: blail@fit.edu (B.A. Lail).

1350-4495/$ - see front matter © 2009 Elsevier B.V. All rights reserved.
doi:10.1016/j.infrared.2009.03.001

2.1. Reciprocity

Lorentz's theorem of reciprocity is given by [5]

$$\int_V (\bar{E}_1 \cdot \bar{J}_2 + \bar{H}_2 \cdot \bar{M}_1 - \bar{E}_2 \cdot \bar{J}_1 - \bar{H}_1 \cdot \bar{M}_2) dV' = -\oint_S (\bar{E}_1 \times \bar{H}_2 - \bar{E}_2 \times \bar{H}_1) \cdot d\bar{s}' \quad (1)$$

where surface S encloses volume V, including inhomogeneous media. Let $\bar{J}_1, \bar{M}_1, \bar{E}_1$, and $\bar{H}_1$ represent the currents and fields of the dipole residing on the interface, while $\bar{J}_2, \bar{M}_2, \bar{E}_2$, and $\bar{H}_2$ correspond to a test dipole. Applying Lorentz reciprocity over all space by considering a sphere of infinite radius, the surface integral of Eq. (1) vanishes, and with no magnetic sources, $\bar{M}_1 = \bar{M}_2 = 0$, we are left with

$$\int_V (\bar{E}_1 \cdot \bar{J}_2) dV' = \int_V (\bar{E}_2 \cdot \bar{J}_1) dV' \quad (2)$$

An ideal dipole carrying current I_1 produces field E_1 at the location of the test dipole I_2. In turn, I_2 produces E_2 at the location of I_1. As shown in Fig. 1, I_1 is the dipole on the air/dielectric interface and I_2 is located in the surrounding regions. Treating I_2 as a test dipole, we will first place it in the air half-space, then on the lens side, to consider the patterns from I_1 in the two half-spaces. If we let $I_1 = I_2 = I$, then we have

$$\int_V (\bar{E}_1 \cdot \bar{I}) dV' = \int (\bar{E}_2 \cdot \bar{I}) dV' \quad (3)$$

Therefore $\bar{E}_1 = \bar{E}_2$. If we can calculate the field E_2 at the location of I_1, then we know the value of E_1 at the test location. $\bar{E}_2$ is the field from the test source multiplied by the coefficient for transmission from the test source region through the flat surface of the lens. For lens-side the test field must transmit from region 0 to region 2 with transmission coefficient τ^{02} whereas for air-side the field is transmitted from region 2 to region 1 with coefficient τ^{21}.

The test source is an ideal dipole of length L oriented as shown in Fig. 2 at the origin of source coordinates (x_s, y_s, z_s). The observation point $P_t(r, \theta_S, \phi_S)$ is the center of the flat boundary between air and the lens. The electric field magnitude due to the test source observed at point $P_t(r, \theta_S, \phi_S)$ is given by

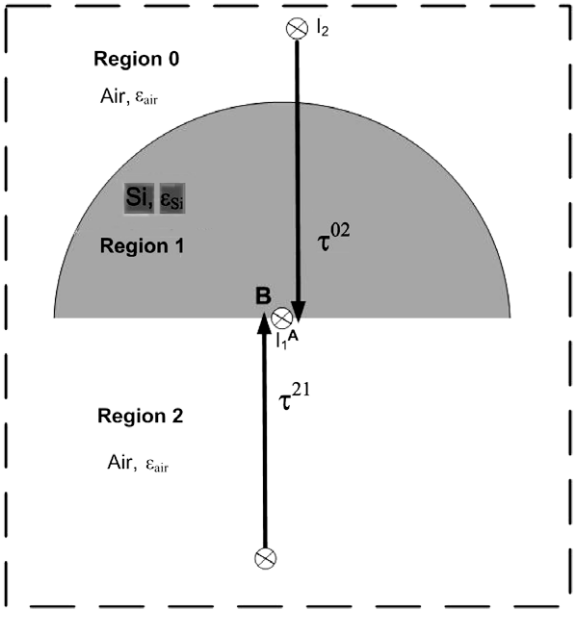

Fig. 1. Lens regions and broadside test dipole locations.

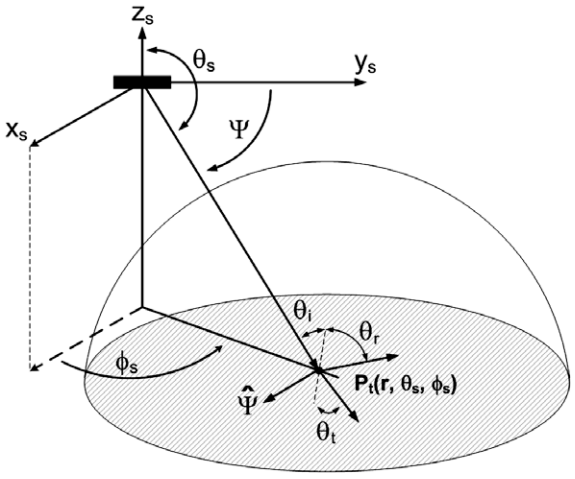

Fig. 2. Immersion lens geometry for reciprocity showing the test dipole location at the origin of coordinates (x_s, y_s, z_s).

$$E_2 = \frac{j\eta k I L}{4\pi r} e^{-jkr} \sin\Psi \quad (4)$$

where η is the intrinsic impedance of the medium, $\sin\Psi = \sqrt{1 - \sin^2\theta_S \sin^2\phi_S}$ and the field is in the $\hat{\Psi}$ direction. The electric field is broken into components parallel and perpendicular to the plane of incidence, which is defined by the angle ϕ_s. By reciprocity, the parallel and perpendicular components of the dipole at location $P_t(r, \theta_s, \phi_s)$ are given by the incident test field multiplied by transmission coefficients $\tau_{//}$ and $\tau_{\perp}$, respectively. Applying reciprocity once more we predict received irradiance (Watt/cm^2) from direction (θ_s, ϕ_s) for air-side illumination and lens-side illumination.

$$S_{air} = \frac{1}{2\eta_o} \frac{|\tau_{\perp}^{21} E_{2\perp} \cos\phi_S|^2 + |\tau_{//}^{21} E_{2//} \cos\theta_r \sin\phi_S|^2}{1 - 2(\sin\phi_S \cos\phi_S)^2} \quad (5)$$

$$S_{lens} = \frac{1}{2\eta_o} \frac{|\tau_{\perp}^{02} E_{2\perp} \cos\phi_S|^2 + |\tau_{//}^{02} E_{2//} \cos\theta_r \sin\phi_S|^2}{1 - 2(\sin\phi_S \cos\phi_S)^2}$$

Here η_o is the intrinsic impedance of free space and θ_r is the refracted angle of the test field at the lens flat surface for each case; from air to Si for S_{air} and from Si to air for S_{lens}. The terms $\cos\varphi_S$ and $\cos\theta_r \sin\varphi_S$ give the component of the electric field parallel to the dipole, and the factor $1–2(\sin\varphi_S \cos\varphi_S)^2$ is for normalization.

2.2. Broadside response

Before continuing we discuss the special case of broadside radiation. Specifically we are interested in the response due to incident field from the $\pm z$ direction. For this case Eq. (5) simplifies to

$$S_{air} = \frac{1}{2\eta_o} |\tau^{21} E_2|^2 \quad (6)$$

$$S_{lens} = \frac{1}{2\eta_o} |\tau^{02} E_2|^2 \quad (7)$$

Assuming the same spot size in the device plane for both air-side and lens-side illumination this gives the power division ratio as

$$\frac{\Phi_{lens}}{\Phi_{air}} = \frac{|\tau^{02}|^2}{|\tau^{21}|^2} \quad (8)$$

Next, we establish the relationship between the steady-state transmission coefficients from air into the Si lens, τ^{21}, and for transmission through the lens, τ^{02}.

Consider Fig. 1, where the broadside transmission paths are shown. On the lens side, the test field must transmit from the air outside the lens (region 0) through the lens and into the air-side (region 2) designated as location A, with steady-state transmission coefficient τ^{02}, which has the general angle-dependent form

$$\tau^{02} = \frac{\tau_{01}\tau_{12}(\theta_i)e^{-jka}}{1+\Gamma_{01}\Gamma_{21}(\theta_i)e^{-j2ka}} \tag{9}$$

Here τ_{01} and Γ_{01} are the Fresnel transmission and reflection coefficients, respectively, for fields from region 0 incident on the curved air/Si boundary, while $\tau_{21}(\theta)$ and $\Gamma_{21}(\theta)$ are Fresnel transmission and reflection coefficients, respectively, for fields from region 2 incident on the flat Si/air boundary. Note that we consider the dipole location to be the center of the flat surface of the lens, so that incident rays directed toward that location are normal to the curved surface. This simplifies the expressions for the curved-surface Fresnel coefficients. However, the Fresnel coefficients at the flat surface are dependent on both the angle of incidence and the wave polarization. For consideration of the air-side fields, the test field is transmitted from the air (region 2) into the lens (region 1) designated as location B, with steady state transmission coefficient τ^{21}.

Let us first consider a high-F/# broadside illumination such that the curved surface can be approximated as flat over the small incident cone angle. Therefore, the lens behaves as a dielectric slab. Power considerations relate the steady state coefficients τ^{21} and τ^{02}. The power reaching locations A and B are given by

$$\Phi_A = \frac{|\tau^{02}|^2|E_o|^2}{2\eta_2}\Delta, \quad \Phi_B = \frac{|\tau^{21}|^2|E_o|^2}{2\eta_1}\Delta \tag{10}$$

where E_o is the incident electric field amplitude, and Δ is a unit area at each location. In a transient analysis, some portion of the incident field enters the dielectric and propagates to the Si/air boundary where it is partially reflected and partially transmitted out of the slab. The portion that is reflected propagates back to the first boundary where a portion of it exits on the front side of the slab while some is reflected again. This process of subsequent boundary interactions continues until steady-state is reached where a fraction of the incident wave is reflected from the front surface, and a fraction is transmitted through the second surface. Energy conservation requires that the steady-state power transmitted into the first boundary of the slab be transmitted out of the second boundary. This requires that $\Phi_A = \Phi_B$ which, from Eq. (10), gives

$$|\tau^{21}|^2 = \frac{\eta_{Si}}{\eta_{air}}|\tau^{02}|^2 \tag{11}$$

Thus, for the case of high-F/# broadside illumination, we find

$$\frac{\Phi_{lens}}{\Phi_{air}} = \frac{|\tau^{02}|^2}{|\tau^{21}|^2} = \frac{\eta_{air}}{\eta_{Si}} = \sqrt{\varepsilon_{r,Si}} \tag{12}$$

Here η_{Si} and η_{air} represent the intrinsic impedance of silicon and air, respectively. Note that this broadside power division ratio Φ_{lens}/Φ_{air} is given by the square root of the lens dielectric constant (the refractive index) and is independent of lens radius. Fig. 3 is a plot of both broadside powers Φ_{lens} and Φ_{air} for a lens of integer half-wavelength radius as a function of the change in lens radius, ΔR, as well as each power averaged over radius, normalized to the average air-side power for both air-side and lens-side illumination. While the broadside power on each side of the plane interface varies with lens radius, the ratio Φ_{lens}/Φ_{air} is constant. The peak in broadside power for both lens-side and air-side occurs for lens radius equal to integer multiples of half wavelength. These properties are exhibited by powers on lens-side/air-side varying as transmission through/into the lens. One might say that the incident wave has better impedance matching from the lens side for all lens radii, and that this impedance match is maximal when the lens radius is an integer multiple of half-wavelength. For half-wavelength radius there is total transmission through the lens, which corresponds to a peak in the lens-side power. There is also a peak in transmission into the lens, which corresponds to peak air-side power. Note that the maximum response from air-side illumination has the same value as the minimum response from lens-side illumination, since $|\tau^{02}(a = \lambda/4)| = |\tau^{21}(a = \lambda/2)|$, where a is the lens radius.

Eqs. (9) and (11) are based on the assumption of a lens of lossless dielectric. In order to determine the amount of absorption a

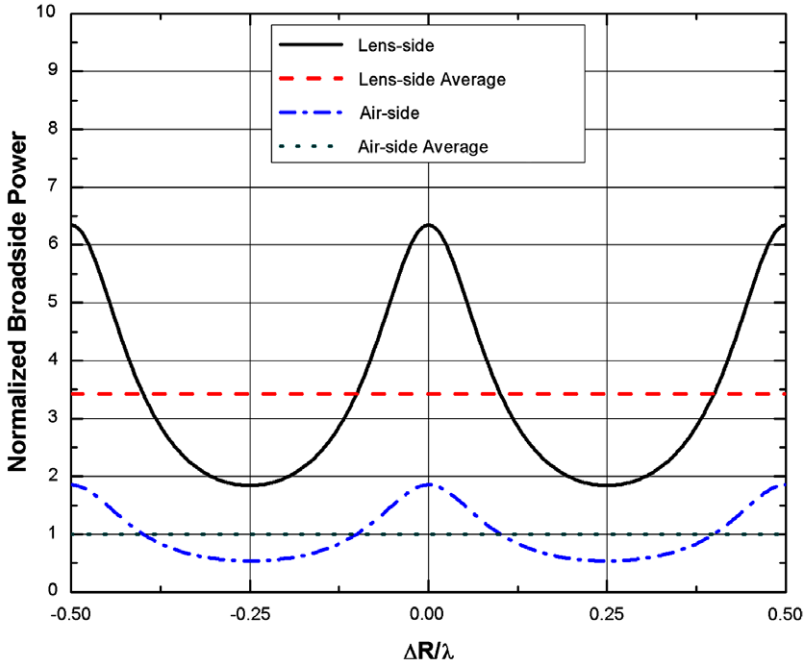

Fig. 3. Plots of Φ_{lens} and Φ_{air} as a function of variation in lens radius; also Φ_{lens} and Φ_{air} averaged over lens radius, for a hemispherical lens of integer half-wavelength. The powers are calculated for the special conditions of large F/# and normal incidence. The plots shown are normalized to the radius-averaged value of Φ_{air}.

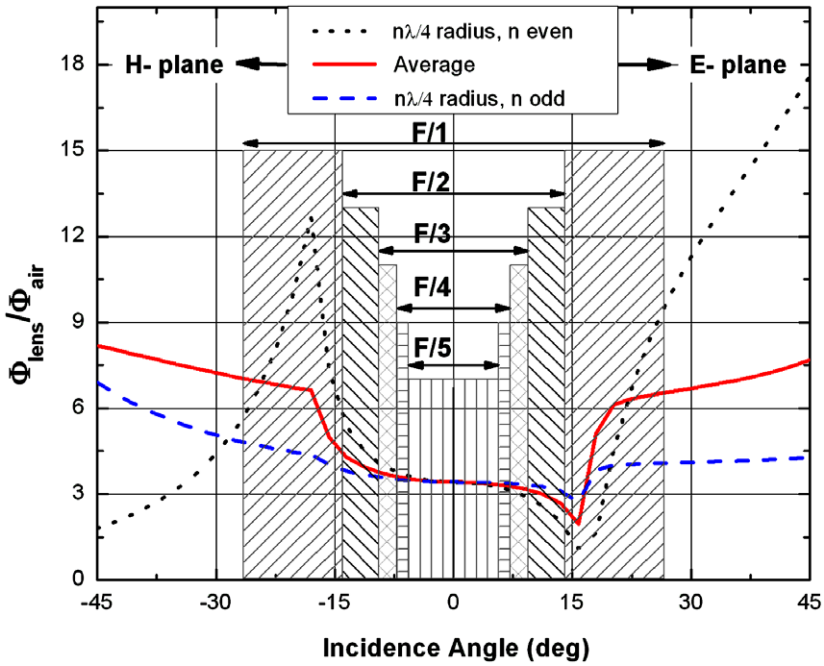

Fig. 4. E-plane and H-plane power ratios Φ_{lens}/Φ_{air} as a function of incidence angle, for a Si immersion lens. The reference F/#s shown are centered on the broadside direction.

high-resistivity Si immersion lens was polished flat to an approximate thickness of 2.5 mm and transmission properties were measured using an IR ellipsometer. The real and imaginary index of refraction measured at 10.6 μm are $n = 3.4193$ and $k = 2.25 \times 10^{-6}$. Calculating the absorption coefficient α as,

$$\alpha = \frac{4\pi k}{\lambda} \tag{13}$$

we obtain $\alpha = 2.67\ \mathrm{m}^{-1}$.

Using Beer's absorption law to calculate the power loss through the lens as

$$\frac{\Phi(z)}{\Phi_0} = e^{-\alpha z} \tag{14}$$

with an immersion lens thickness (radius) of 5 mm results in a negligible power loss of 1.3%.

2.3. Off-axis response

In the previous section the power division between lens-side and air-side broadside illumination was shown to be independent of lens radius. As we consider off-axis response this is no longer true. The steady state transmission coefficients are dependent on both angle of incidence and lens radius. Furthermore, the transmission coefficients are dependent on wave polarization and are presented in terms of electric field components parallel and perpendicular to the plane of incidence.

In this study, a nominally 5-mm Si lens is used. Given a 10.6-μm illumination wavelength, the wavelength in the lens is $\lambda_{Si} = 3.1$ μm. In order for the tolerance of lens radius to be a single wavelength, a fabrication accuracy of 0.06% would be required. The manufacturer-specified tolerance on the lens radius is 1%. This means that the observed response is likely not due to a specific lens radius, but is an average over lens radii. The powers on the lens- and air-side of the plane interface have been formulated in terms of the transmission coefficients τ^{21} and τ^{02}, with the dependence on lens radius shown in Eqs. (9) and (11). This results in a periodic response as a function of radius. Therefore, we can find the average over radius by integration.

$$\Phi_{ave}(\theta,\phi) = \frac{1}{a}\int_0^a \Phi(\theta,\phi,a)da \tag{15}$$

With the same medium on both sides of the lens, both air-side and lens-side response are periodic in radius with minima at odd multiples of quarter-wavelength and maxima at even multiples. This periodicity is seen for the broadside case in Fig. 3, and it should be noted that the periodicity is maintained for off-axis illumination.

The off-axis power ratio Φ_{lens}/Φ_{air} is also periodic in lens radius. The predicted power ratio Φ_{lens}/Φ_{air} is plotted in Fig. 4 for both the E-plane and H-plane patterns. Results for radii of even and odd multiples of quarter wavelength, as well as the ratio averaged over lens radius, are presented. The range of incidence angles corresponding to various F/#s are noted, centered on the broadside direction. The power ratio for large F/# for which the off-axis features do not alter the response is the same as seen in Fig. 3. However, as F/# is decreased to F/1 the off-axis features enter the illumination cone-angle and must be accounted for in predicted power division. As F/# is varied the total power density (irradiance) in the device plane is found by integrating over the cone solid angle.

3. Measurements

In order to obtain experimental data a single dipole antenna was fabricated at the center on the flat side of a high resistivity Si immersion lens as shown in Fig. 5 [4]. The antenna was designed to be resonant for 10.6 μm radiation. The material of the antenna is gold (Au) of 150 nm thickness. A nickel (Ni) microbolometer of 100 nm thickness is placed at the antenna feed point and the signal (the dc voltage response of the bolometer) is read out with Au lead lines.

The lead lines are routed perpendicular to the antenna to reduce effects of the lead lines picking up the incident radiation. A CO_2 laser operating at a wavelength of 10.6 μm was used as the source. A wire grid polarizer was used in conjunction with a half-wave plate in order to control the polarization state of the radiation. For the radiation pattern measurements, an F/8 optical system was used to focus the laser onto the detector consisting of the antenna

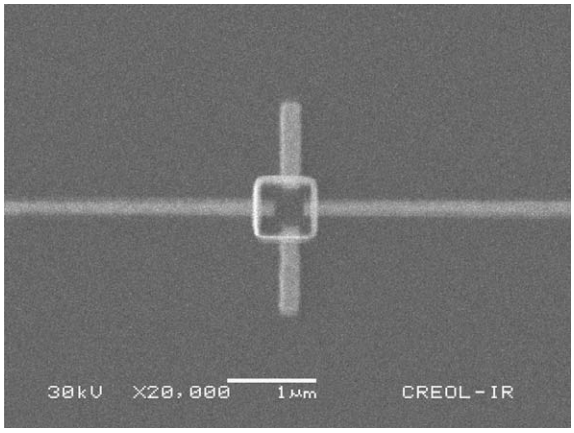

Fig. 5. Au dipole antenna and lead lines with a Ni bolometer on Si immersion lens.

coupled bolometer and the hemispherical silicon lens. The beam diameter at the F/8 focusing lens was measured to be 12 mm. At the curved surface of the hemispherical side of the silicon lens, the beam diameter was 400 μm. The use of a high F/# system reduces the convolution of the beam focus cone with the angular antenna pattern. A mechanical chopper was used to modulate the laser at 2.5 kHz. The antenna was biased at 100 mV DC. A lock in amplifier was used in conjunction with a computer using LABVIEW to record the output signal of the device. The hemispherical silicon lens with the antenna coupled bolometer located at the center of its flat surface was mounted in a 5-axis goniometer which was used to place the detector at the focus of the illumination beam. This setup allowed the antenna to rotate in azimuth and elevation around this point.

The optical setup was modified to measure the device's response as a function of illumination F/# by replacing the focusing lens with a F/1 lens. A variable aperture was inserted directly in front of the lens to allow changing of the system F/# without the need for repositioning of the device. The antenna was mounted on a nano-mover controlled stage to allow precise positioning of the device with respect to the laser focus.

4. Results

Measured and predicted normalized (to lens-side maximum) radiation patterns for the E-plane, H-plane, and a cut plane at $\phi = 45^{o}$ for lens-side and air-side illuminations are shown in Fig. 6. Predicted local irradiance in the device plane as a function of incidence angle is plotted, which is equivalent to a power pattern through the fact that effective area of the antenna is a function of angle. Predictions agree very well with measurements in the key features of the angular pattern. The E-plane has a null at the critical angle whereas the H-plane peaks. The 45-degree cut plane is midway between the E- and H-planes. The broadside power ratio, Φ_{lens}/Φ_{air}, is consistent with predictions in all three cut-plane measurements.

The ratio of lens-side to air-side irradiance responsivity as a function of illumination F/# for illumination centered on the broadside direction is presented in Fig. 7. Three predicted curves are plotted corresponding to lens radius of even (maximum

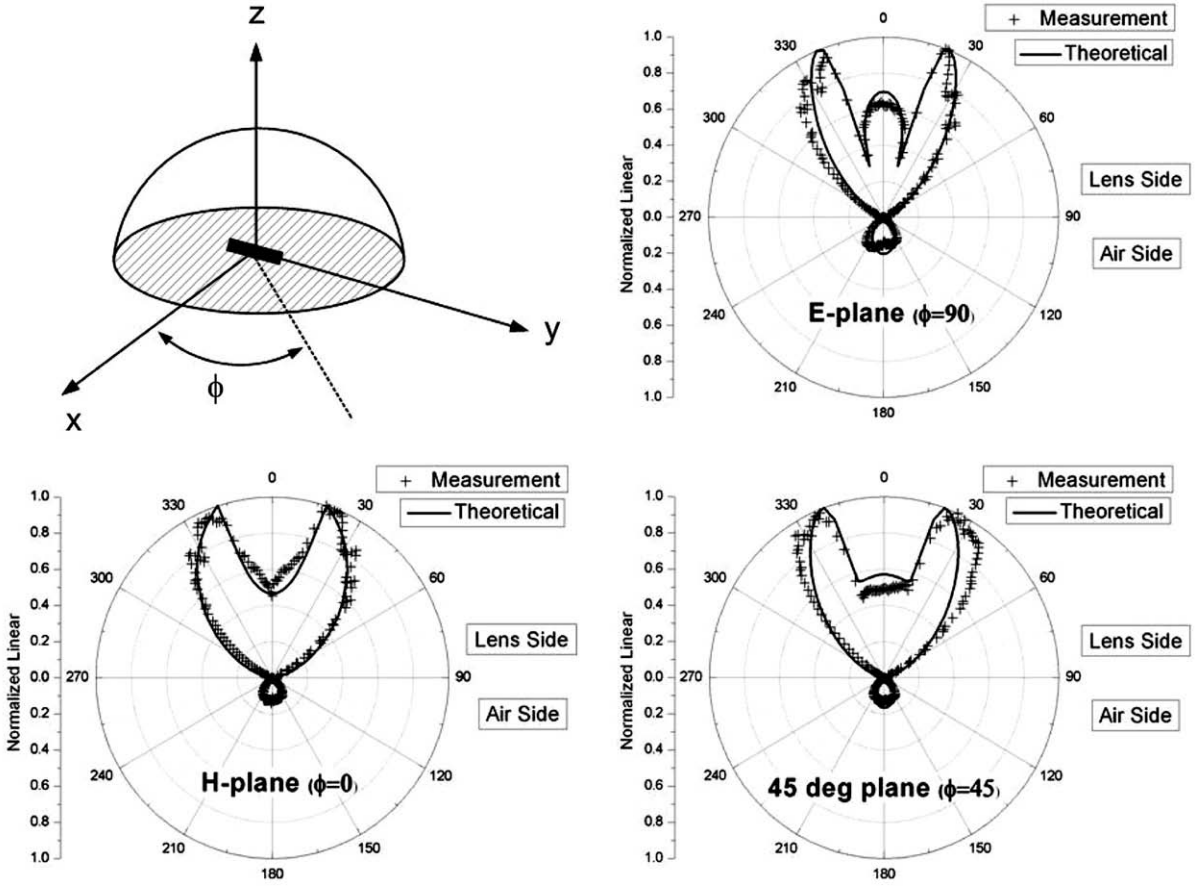

Fig. 6. Angle-dependent power patterns for E-plane, H-plane and 45-degree plane – comparison of theory and experiments.

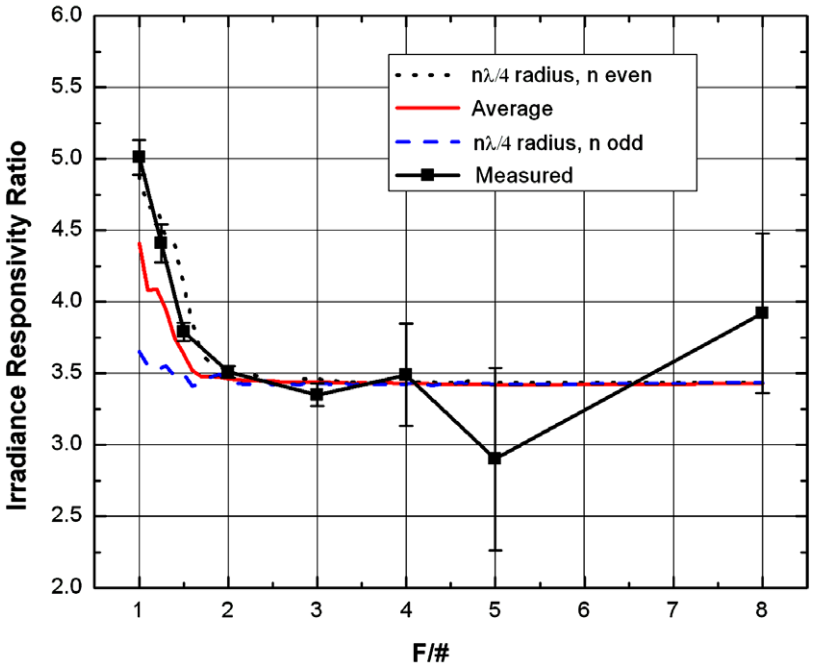

Fig. 7. Ratio of lens-side to air-side irradiance responsivity (V cm^2/W) as a function of F/# for illumination centered at broadside.

response) and odd (minimum response) multiples of quarter-wavelength as well as the average in radius. For F/# greater than F/2 the predicted power ratio is constant with value 3.42. Measured values exhibit similar behavior. Each measured data point represents the average of 20–40 measurements and error bars represent the standard deviation in the measured data. The measurement of the irradiance response is accomplished by decreasing the size of a variable aperture in front of the last lens. As the F/# was increased the power illuminating the antenna is reduced, and due to diffraction the beam's spot size increased resulting in a reduction of the irradiance in the antenna aperture plane. This was mitigated by increasing the laser's output power. For the measurements done at large F/#s, the laser was set to maximum output and measurements were completed at a decreasing signal-to-noise ratio, resulting in larger fluctuations in the measurements as indicated by the increase in the size of the error bars. As F/# is reduced to F/1, the power ratio increases due to off-axis contributions.

In Fig. 8 the pertinent geometry for characterizing the device broadside response as a function of F/# is shown. Note that here F/# refers to the illuminating system prior to the hemispherical surface. Illumination F/# is given by F/D, where F is the focal length and D is the diameter of the lens. Therefore, F/# can be changed by varying either F or D while holding the other fixed. Here A_{cone} is the illuminated area of the lens corresponding to diameter D given by $A_{cone} = \pi(D/2)^2 = \pi[F/(2\ F/\#)]^2$. A_{spot} is the area of the focused spot. For diffraction-limited spot size $A_{spot} = \pi(1.22\ \lambda\ F/\#)^2$. The irradiance in A_{cone} will be considered a constant. Also, we assume that the total power in A_{spot} is equal to the total power in A_{cone}. Results are presented in terms of irradiance responsivity with reference to the irradiance in Acone. In other words, we plot the device response as a function of F/# for constant irradiance incident on the lens. Plots are normalized to air-side F/1 response.

Irradiance responsivity as a function of F/# with D varied while F is held constant is shown in Fig. 9 for both lens side and air side. The total power entering the cone angle is a product of incident irradiance and A_{cone}, which varies as $(F/\#)^{-2}$. Keeping in mind that the power in A_{spot} is the same as the power in A_{cone}, and noting that A_{spot} varies as $(F/\#)^2$, we get a local irradiance in the spot which varies as $(F/\#)^{-4}$, hence the steep falloff in response as a function

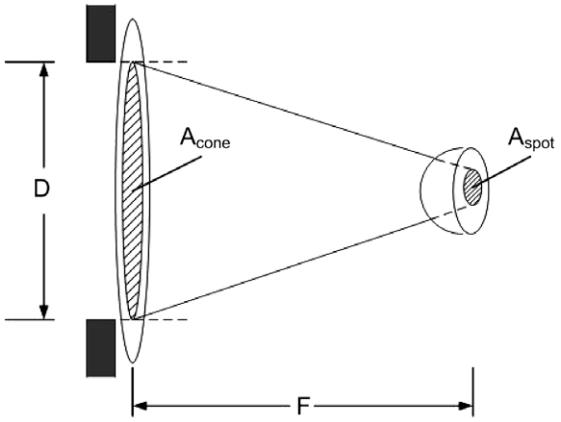

Fig. 8. Pupil plane and image plane geometry for varying F/#.

of increasing F/#. Fig. 10 is a plot of irradiance responsivity as a function of F/#, but now D is held fixed and F is varied. Since A_{cone} is held constant in this case, total power in both A_{cone} and A_{spot} are fixed as a function of F/# and the local irradiance illuminating the spot now varies as $(F/\#)^{-2}$. This explains the slower falloff as a function of F/# in Fig. 10 as compared to that of Fig. 9. The two key factors evident in the response as a function of F/# are the response ratio, Φ_{lens}/Φ_{air}, and the local irradiance illuminating the device. The illumination radiometry dictate the falloff in local irradiance as F/# is varied, as described above, while the response ratios of Fig. 7 are maintained at each F/#.

Measured responses as a function of F/# correspond to varied D with F fixed. Both device response (volts) and total power in the spot were measured. Knowing the lens illumination diameter D, irradiance responsivity in V/(W/cm^2), with reference to irradiance in A_{cone}, are plotted in Figs. 9 and 10. Since the total power in both A_{cone} and A_{spot} is a constant as a function of F/#, Fig. 10 is also a plot of responsivity in V/W. Predicted response is obtained by integrating over the cone solid angle at each F/#. This yields a response per

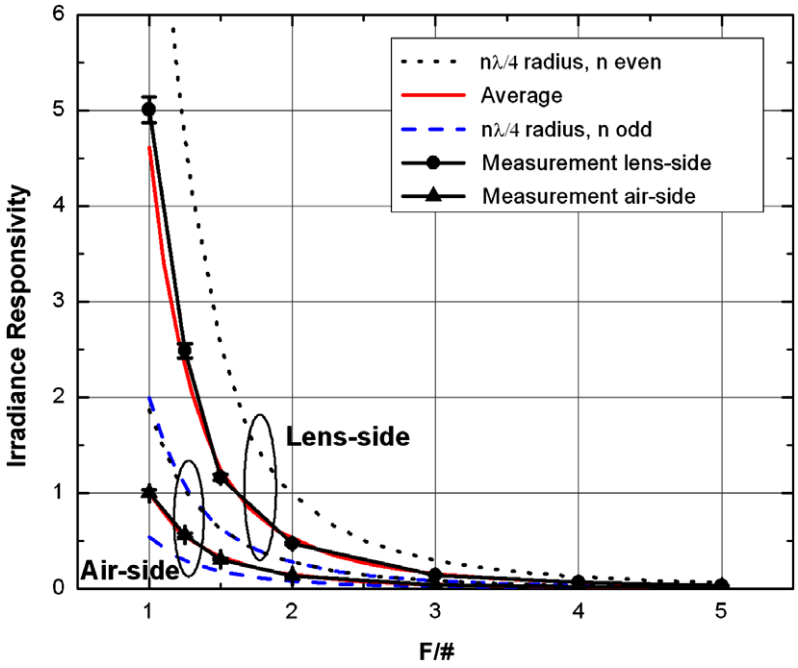

Fig. 9. Irradiance responsivity (V cm^2/W) normalized to air-side F/1 irradiance responsivity as a function of illumination F/# as D is varied and F constant for illumination centered at broadside.

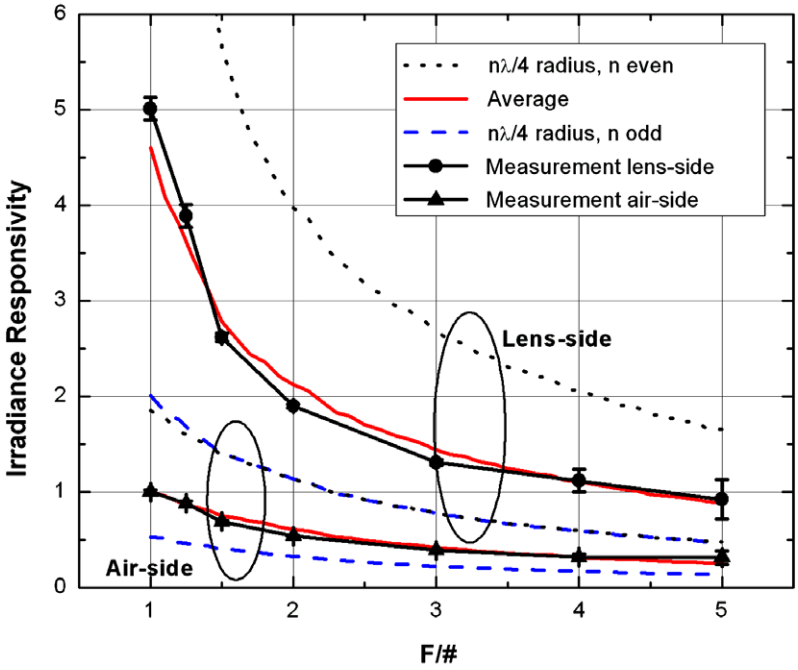

Fig. 10. Irradiance responsivity (V cm^2/W) normalized to air-side F/1 irradiance responsivity as a function of illumination F/# as D is constant and F varied for illumination centered at broadside.

total illumination power, which is presented as irradiance responsivity by normalizing to A_{cone} in each case.

The ratio between the lens-side and air-side responses has been seen to be on average equal to the index of refraction of the lens element. This arises from the Fabry-Perot interactions between the lens surfaces, and falls short of the $\varepsilon^{3/2}$ prediction if one had a dielectric half space. This ideal condition may however be approximated by the use of an antireflection (AR) coated hemispherical lens. For a perfect AR coating, the reflection coefficient from the curved surface would be zero and the situation would be analogous to a half space. To test this idea, we were able to deposit a thin (approximately 1 micrometer) coating of benzocyclobutene (BCB) onto the pole of the curved surface. Although not a perfect AR coating, this increased the lens-side to air-side ratio from 3.4 (uncoated) to 6.7 (coated) for the device reported on in this paper. Such coatings hold promise for further increases in responsivity. For instance, a Ge lens with perfect AR coating would have a factor of 64 higher broadside response from the lens side than from the air side.

In order to better characterize the potential improvement from an ideal AR coating we integrate patterns over cone angles for the limiting cases F/∞ and F/0, corresponding to responses from

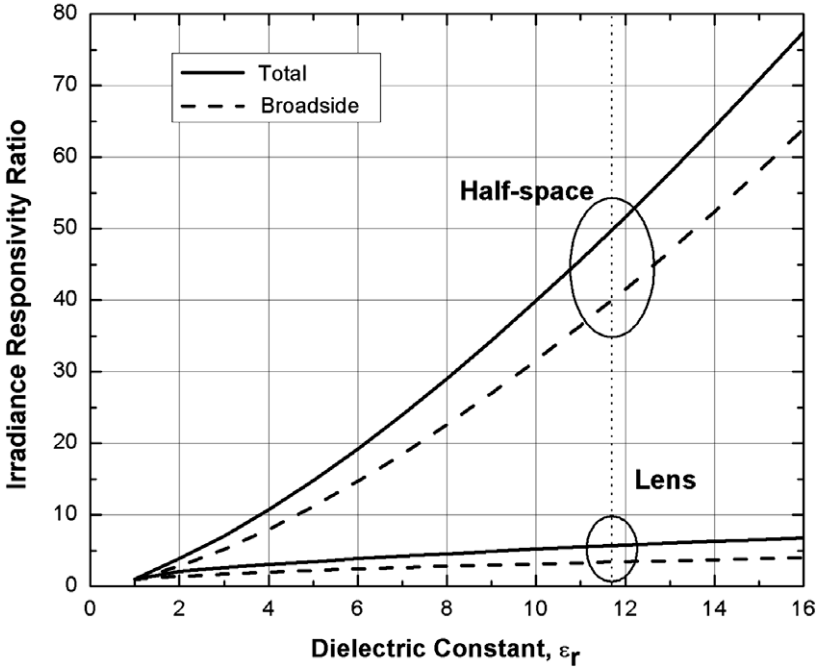

Fig. 11. Total and broadside dipole irradiance responsivity ratio of dielectric (lens) side to air side as a function of dielectric constant.

broadside illumination and total response from the entire illumination half-space, respectively. Predicted broadside and total response ratio as a function of dielectric constant, for both the lens case and the half-space formulation (ideal AR coating), are shown in Fig. 11. At broadside the half-space response ratio varies as $\varepsilon^{3/2}$ while the lens response ratio varies as $\varepsilon^{1/2}$. As the cone angle is increased to include illumination over the full half space of the receiving side, the response ratio increases due to off-axis features in the angular patterns. For Si the ratio increases from 40 (broadside) to 50 (total) and for Ge the ratio increases from 64 (broadside) to 77 (total).

5. Conclusion

The air-side and substrate-side responses of a dipole antenna on a hemispherical Si lens have been theoretically and experimentally investigated at $\lambda = 10.6$ μm. A formulation based on reciprocity that predicts the response as a function of incidence angle for lens-side and air-side is presented. Fabry–Perot effects give rise to response which is periodic in lens radius. The lens considered is nominally 5 mm in radius, which is electrically large, and considering fabrication tolerances it is expected that observed response is due to an average over lens radius. The ratio of broadside responses, Φ_{lens} and Φ_{air}, are shown to be periodic in radius but with a constant ratio Φ_{lens}/Φ_{air} given by the dielectric constant of the lens, 3.4 for Si. Off-axis response must be accounted for in predicting the power ratio for low F/#. Angular patterns for E- and H-planes, as well as a 45° cut plane are presented with good agreement between predictions and measurements. The broadside power ratio, Φ_{lens}/Φ_{air}, has a value of 5 for F/1 illumination, but decreases and remains constant at a value of 3.4 as F/# is increased above F/2. Broadside device response as a function of F/# (=F/D) maintains the ratio Φ_{lens}/Φ_{air} while responding to incident irradiance. Variation of F/# is achieved by varying either F or D while holding the other fixed. Local irradiance illuminating the device goes as $(F/\#)^{-4}$ when D is varied, and as $(F/\#)^{-2}$ when F is varied. Response ratios of a dipole on the dielectric hemispherical lens are compared to those of dipole at the boundary of a dielectric half-space (ideal AR coated lens) as a function of dielectric constant. The broadside responses vary as $\varepsilon^{1/2}$ for the lens and $\varepsilon^{3/2}$ for the half-space dielectric, respectively, and increase as the illumination cone-angle is broadened to include the entire receiving half-space.

References

[1] J. Alda, C. Fumeaux, M. Gritz, D. Spencer, G.D. Boreman, Responsivity of infrared antenna-coupled microbolometers for air side and substrate-side illumination, Infrared Physics and Technology 41 (2000) 1–9.
[2] C.R. Brewitt-Taylor, D.J. Guntun, H.D. Rees, Planar antennas on a dielectric surface, Electronics Letters 17 (20) (1981) 729–731.
[3] D.B. Rutledge, D.P. Neikirk, D.P. Kasilingam, Integrated-circuit antennas, Infrared and Millimeter Waves 10 (1983) 1–90.
[4] C.T. Middlebrook, G. Zummo, G.D. Boreman, Direct-write electron-beam lithography of an IR antenna-coupled microbolometer onto the surfaceof a hemispherical lens, Journal of Vaccum Science and Technololgy B 24 (6) (2006) 2566–2569.
[5] C. Balanis, Advanced Engineering Electromagnetics, John Wiley & Sons Inc., 1989.